Linear and nonlinear microwave properties of Ca-doped YBa2Cu3O7−δ thin films

D. Seron, D. E. Oates, German Hammerl, Jochen Mannhart, P. J. Hirst, R. G. Humphreys, A. C. Anderson, M. A. Hein, J. Derov

Angaben zur Veröffentlichung / Publication details:

Seron, D., D. E. Oates, German Hammerl, Jochen Mannhart, P. J. Hirst, R. G. Humphreys, A. C. Anderson, M. A. Hein, and J. Derov. 2005. "Linear and nonlinear microwave properties of Ca-doped YBa2Cu3O7−δ thin films." *Physical Review B* 72 (10): 104511. https://doi.org/10.1103/physrevb.72.104511.

Linear and nonlinear microwave properties of Ca-doped $YBa_2Cu_3O_{7-\delta}$ thin films

D. Seron,[1] D. E. Oates,[2] G. Hammerl,[3] J. Mannhart,[3] P. J. Hirst,[4] R. G. Humphreys,[4] A. C. Anderson,[2] M. A. Hein,[5] and J. Derov[6]

[1]*MIT Department of EECS, Cambridge, Massachusetts 02139-4301, USA*

[2]*MIT Lincoln Laboratory, Massachusetts Institute of Technology, Lexington, Massachusetts 02420-9108, USA*

[3]*Experimentalphysik, 6, Institute of Physics, University of Augsburg, Germany*

[4]*QinetiQ, Malvern, United Kingdom*

[5]*Faculty for Electrical Engineering and Information Technology, Technical University of Ilmenau, 98684 Ilmenau, Germany*

[6]*AFRL/SNHA, Hanscom AFB, Bedford, Massachusetts 01731, USA*

(Received 7 June 2004; revised manuscript received 21 July 2005; published 14 September 2005)

The microwave properties of Ca-doped YBaCuO (YBCO) thin films ($350\ \text{nm} \leqslant t \leqslant 400\ \text{nm}$) have been investigated, using 30% Ca-substituted YBCO ($Y_{0.7}Ca_{0.3}Ba_2Cu_3O_{7-\delta}$) surface layers, as such layers have been shown to enhance the critical-current density of films with high-angle grain boundaries for dc and low-frequency currents. This study is an extension to the microwave range, with the aim of obtaining conditions that improve the transport properties of high-temperature superconductors. The effect of the substitution was observed to be dependent on the thickness of the overlayer. A small but significant improvement in the nonlinear part of the surface impedance (Z_s) and intermodulation distortion (IMD) was observed for a sample with a 20-nm-thick $Y_{0.7}Ca_{0.3}Ba_2Cu_3O_{7-\delta}$ surface layer. These results indicate that some potential exists to improve the nonlinear microwave properties by Ca substitution. On the other hand, samples with a 40-nm-thick $Y_{0.7}Ca_{0.3}Ba_2Cu_3O_{7-\delta}$ surface layer exhibit a degradation of their microwave properties. The possible causes of improvement and degradation are presented in view of the deposition procedure and the oxygen content of the films.

DOI: 10.1103/PhysRevB.72.104511 PACS number(s): 74.25.Nf, 74.78.Bz, 74.78.Fk

I. INTRODUCTION

The high-temperature superconductors (HTS) have found an application as receive filters. However, the nonlinear behavior of HTS at microwave frequencies is still a limitation to wider applications. Even at relatively low microwave power, nonlinear characteristics can generate intermodulation distortion (IMD) in a filter.[1] To investigate the origin of the nonlinearities and to improve the microwave power-handling capability of HTS thin films, substitution with calcium has been investigated and is reported here.

Ca substitution has already been shown to enhance the critical-current density j_c of coated-conductor films for dc or low-frequency power distribution.[2] The enhanced j_c results from diffusion of Ca atoms along high-angle grain boundaries (GB)[3] that improves the intergranular critical current density j_{cJ}. Even in high-quality epitaxial films, since GBs might be sources of losses and nonlinear effects at microwave frequencies, enhancement of the properties might be expected from Ca doping.

The substitution is accomplished using a 30% Ca-rich ($Y_{0.7}Ca_{0.3}Ba_2Cu_3O_{7-\delta}$) surface layer. The results from surface impedance $Z_s(T, I_{rf})$ and intermodulation distortion (IMD) measurements are presented here. The Z_s and IMD are dependent on the thickness of the overlayers, which is in good agreement with dc and ac transport properties and low-power Z_s measurements. A small improvement of the nonlinear properties was achievable under certain conditions that are discussed in this paper. An analysis that takes into account the growth process of the samples and the oxygen content is proposed. The effects of the different surface processes are also described and are helpful to extract the role of the Ca doping.

II. GENERALITIES OF Ca DOPING

A. Substitution in a YBCO single crystal

Overdoping is a way to improve the transport properties and thus to increase the critical current density j_c. Substitution by acceptor ions such as Ca^{2+} or overdoping by oxygen is a way to increase the hole concentration and obtain higher j_c values. Replacing Y^{3+} by Ca^{2+} effectively introduces one additional hole per substituted atom.[4,5] Ca substitution is accompanied by an increase in oxygen vacancies and disorder that partially compensate the hole generation effect.[4] Because of its larger ionic diameter than Y, Ca acts like a hydrostatic pressure and induces a deformation of the CuO_2 planes[6] that also affects the apical oxygen[7] and the Ba site.[8] It has also been shown that for doping levels exceeding 11%, Ca can also substitute for Ba (Ref. 8) via CaO nucleation and BaO desorption,[9] yielding disorder in the CuO chains and degrading the superconducting properties of the YBCO. As shown by Kucera and Bravman,[10] a partial recovery of the critical temperature can be obtained after oxygen annealing, which compensates for the creation of oxygen vacancies. Annealing is necessary to conserve a high value of the critical current density j_c and good microwave properties, as overdoping in oxygen was shown to be a key factor for a high power-handling capability and low intermodulation at microwave frequencies.[11,12]

B. Doping bulk YBCO and YBCO films using a Ca-substituted surface layer

The intergranular critical-current density j_{cJ} in polycrystalline HTS is an order of magnitude smaller than the intragrain current density j_{cG}. GBs are also known to contribute substantially to losses and nonlinearities in the microwave range.[13,14] Mannhart and Hilgenkamp[15] have used the model of band bending to interpret the reduction of the j_c at the vicinity of a boundary. The properties of the depleted region and of the GBs can be improved by hole doping, aided by the circumstance that Ca atoms preferentially diffuse along the boundary. Berenov *et al.*[16,17] recently calculated the diffusion constant of Ca atoms along GBs and showed that it is of the order of 10^3 times greater than that of YBCO grains, hence making selective doping of the GBs possible. Other authors have also proven an increase of the j_c in the case of low-angle GBs.[18] From transmission electron microscopy, a decrease of the GB barrier potential V_{GB} and spatial extent[19] after Ca substitution were demonstrated, which matches well with the doped-Mott-insulator model describing YBCO. It gives an explanation to the increase of j_{cJ} and the overall j_c of the superconductor. Hammerl *et al.*[20] took advantage of the selective doping of the GBs without reducing the critical temperature, by use of a surface layer substituted with Ca or by YBCO/Y(Ca)BCO superlattices,[20] to achieve large j_{cJ}.

Films for microwave applications have reached a high quality level and any grain boundaries are of a very low angle. Nevertheless, they still contain defects like dislocations and antiphase boundaries. The role of these defects in the nonlinear microwave response is not known, but it is reasonable to presume that Ca diffusion along a dislocation might be comparable to that along a grain boundary. Besides, Berenov *et al.*[17] proposed that Ca diffuses first in defects and then laterally, leading to overdoping of the grains. By analogy with the high-angle grain-boundary case and the effect of O doping,[11] hole doping by Ca diffusion, thereby overdoping the grains, might minimize microwave nonlinearities and is our purpose in this study.

C. Previous investigations of the effects of Ca doping on microwave properties

Lorenz *et al.*[21] characterized YBCO with several levels of homogeneous substitution of Y with Ca. Results were obtained for the linear and nonlinear behavior of large-area $Y_{0.9}Ca_{0.1}Ba_2Cu_3O_{7-\delta}$. In the range from 20 to 50 K, the Ca-substituted film shows better microwave properties for a microwave magnetic field up to 20 mT than a plain YBCO film from the same deposition process. The surface resistance is lower in the low-field region for the Ca-doped film. However, upon increasing the microwave magnetic field above 20 mT, the substituted film exhibits larger nonlinearities than the plain YBCO film at all temperatures.

Characterization of the linear surface resistance of a YBCO film covered with a 20% Ca-substituted YBCO surface layer ($Y_{0.8}Ca_{0.2}Ba_2Cu_3O_{7-\delta}$) was reported by Obara *et al.*[22,23] Their results show an improvement of the surface resistance that is dependent on the surface-layer thickness. The optimal-thickness layer (40 nm in their study) was found to reduce the linear R_s by 35%. However, if the thickness of the surface layer is larger than 40 nm, the microwave properties deteriorate. Thus, a tradeoff exists between the substitution level of the overlayer and the optimal thickness. This result is consistent with those of Hammerl *et al.*[2] showing the influence of the surface layer thickness on the critical-current density of a symmetrical 24°-tilt-angle GB.

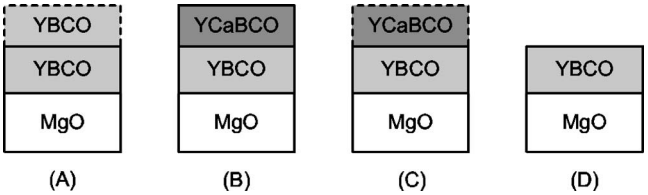

FIG. 1. Schematic description of the films under test. The dashed overlayers were removed by ion-beam etching.

III. FILM PROCESSING AND MICROWAVE CHARACTERIZATION

A. Substrates and deposition process

In the present study, one set of films was deposited onto $LaAlO_3$ substrates and another onto MgO. For the first set, a 400-nm-thick nm thick epitaxial YBCO film was deposited by inverted cylindrical magnetron sputtering[24] onto a 5 cm diameter $LaAlO_3$ wafer, which was subsequently diced to obtain four equivalent 1 cm squares. Two of the four samples were used as baselines and exhibit the same behavior of $Z_s(T, I_{rf})$, within the experimental accuracy. Pulsed-laser deposition (PLD) was then used to deposit a $Y_{0.7}Ca_{0.3}Ba_2Cu_3O_{7-\delta}$ surface layer 20-nm thick on one of the films and a 40-nm thick on another.[20]

The second set consisted of four 350-nm-thick epitaxial films that were grown simultaneously on 1 cm$\times$1 cm homoepitaxially buffered MgO substrates by electron-beam-assisted thermal coevaporation.[25] A postanneal treatment using a plasma-activated oxygen atmosphere was then applied to each sample to ensure full oxygenation. An inductive measurement of T_c and j_c confirmed that at this stage, the four films were very similar [$T_c \sim 89$ K, $j_c(77\ \text{K}) \sim 3 \times 10^6$ A/cm^2). To ascertain the effect of Ca substitution, the procedure[26] presented in Fig. 1 was followed: one film (A) had a 40-nm-thick undoped YBCO surface layer deposited by PLD as a control. This surface layer was then removed by ion etching. A second film (B) was doped using a 40-nm-thick $Y_{0.7}Ca_{0.3}Ba_2Cu_3O_{7-\delta}$ surface layer deposited by PLD. A similar surface layer was also deposited by PLD on the third film (C), but it was then removed by ion etching to obtain information on the diffusion of Ca atoms in the YBCO layer. The fourth film (D), whose bare surface was ion milled, was used as a reference for the behavior of the YBCO layer. As a final step, all films in this set had a second anneal in plasma-activated oxygen[27] to ensure full oxygenation.[11,12]

For both sets of films, the deposition of the surface layer by PLD was done at 760 °C in less than 10 min (Ref. 2). The films were then cooled in an oxygen atmosphere of 0.4 bar

for oxidation. For these values of time, temperature, and film thickness (300 nm$<t<$400 nm), the depth profile reported by Berenov *et al.*[16] predicts that Ca will diffuse in the GBs over the full thickness and then laterally, leading to overdoping of the grains. However, because of the dynamic conditions of the deposition, full quantitative agreement with Berenov's steady-state results might not be obtained.

B. Microwave characterization

All films were patterned by wet etching to obtain stripline resonators for microwave characterization.[28] The samples grown on $LaAlO_3$ have a resonant frequency at 1.5 GHz while those on MgO at 2.3 GHz, due to the different dielectric constants of the substrates.

The resonators are used to measure the surface impedance $Z_s(T, I_{\rm rf})$ as a function of temperature and the circulating microwave current. Low-power microwave measurements allow the extraction of the penetration depth λ and critical temperature.[29] In the frame of the two-fluid model for $\lambda(T)$, we can obtain $\lambda(T=0, I_{rf}=0)$ with 20% accuracy.

To investigate the nonlinear properties in more detail, IMD measurements were then carried out for every resonator by applying two closely spaced frequencies f_1 and f_2 within the 3-dB bandwidth of the resonator. Nonlinear contributions in the surface impedance $Z_s(I_{\rm rf})$ generate third-order mixing products at frequencies $(2f_1-f_2)$ and $(2f_2-f_1)$ and higher-order terms,[13] as well as harmonic terms at nf_1 and nf_2 (Ref. 30). It has been shown analytically that the output power at the IMD products $P_{\rm IMD}(2f_i-f_j)$, $i\neq j$, depends on the nonlinear surface reactance and resistance,[31] and in the simplest approximation is proportional to $P^3_{\rm in}(f_i)$, where $P_{\rm in}$ is the input power. It is given by[32]

$$P_{\rm IMD} = (a_{Xs}^2 + a_{Rs}^2)\frac{[2r_\nu(1-r_\nu)]^4 Q_0^4}{\pi^2 Z_0^4} P_{\rm in}^3, \tag{1}$$

where a_{Xs} and a_{Rs} are defined by $\Delta X_s(I_{\rm rf}) = a_{Xs} I_{\rm rf}^2$ and $R_s(I_{\rm rf}) = R_{s0} + a_{Rs} I_{\rm rf}^2$, r_ν is the voltage ratio between the output and the input that is related to the insertion loss by IL $= 20\log(r_\nu)$, and Z_0 is the characteristic impedance of the resonator.

Experimental results often show that $P_{\rm IMD}(2f_i-f_j)$ scales like $P^n{}_{\rm in}(f_i)$ with $2\leqslant n\leqslant 3$.

To correct for different resonator quality and coupling factors, normalizations have to be carried out on the measured IMD power,[33–36] as presented by Eqs. (1)–(3). In addition, it is preferable to plot the IMD power as a function of the output power $P_{\rm out}(f_i)$ at the input frequency or the circulating power $P_{\rm circ}(f_i)$ defined in Eq. (2). $P_{\rm out}(f_i)$ and $P_{\rm circ}(f_i)$ are proportional to the average current that circulates inside the resonator.

$$P_{\rm circ} = \frac{(1-r_\nu)}{r_\nu \pi} Q_0 P_{\rm out} = \frac{r_\nu(1-r_\nu)}{\pi} Q_0 P_{\rm in}, \tag{2}$$

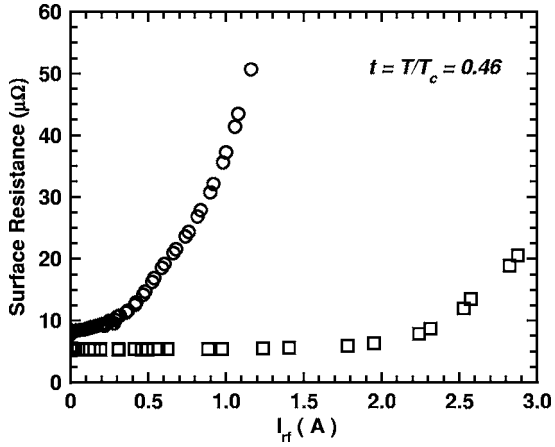

FIG. 2. A comparison at $t=T/T_c=0.46$ between the nonlinear surface resistance $R_s(I_{\rm rf})$ of the baseline sample SP3 on $LaAlO_3$ (circles) with that of the reference sample D on MgO that was annealed (squares). The resonant frequency is 1.5 GHz for SP3 and 2.3 GHz for the sample D.

$$\frac{P_{IMD}}{r_\nu(1-r_\nu)Q_0} \propto (a_{Xs}^2 + a_{Rs}^2) P_{\rm circ}^3. \tag{3}$$

Thus, we normalize the measured $P_{\rm IMD}$ by the measured Q and r_ν as shown in Eq. (3).

IV. COMPARISON BETWEEN NON-Ca-SUBSTITUTED SAMPLES

We compare the nonlinear surface resistance $R_s(I_{\rm rf})$ of the undoped sample after oxygenation (on MgO) with the as-grown samples on $LaAlO_3$ in Fig. 2. The two samples never had any Ca-rich overlayer. The results are presented at one representative temperature, but the measurements were done over the whole range from 4.2 K to the T_c of the samples.

According to their linear R_s and level of IMD, the samples on $LaAlO_3$ were of a lower quality than previously reported for this process.[24] X-ray diffraction revealed the presence of green-phase YBCO ($Y_2Ba_1Cu_1O_5$) in this film. The oxygenated sample remains very linear up to high rf current, close to 2 A. Then the nonlinearity becomes visible and might be the consequence of flux penetration or heating.[37,38] The nonlinearity occurs at a much lower power for the as-grown sample, at $I_{\rm rf}\approx 0.4$ A. This is probably related to a lower j_c or to the presence of defects that diminish the field H_p (Ref. 39), equivalent to the dc field H_{c1} and proportional to $I_{\rm rf}$, yielding an easier vortex penetration. Local heating can also be responsible for this difference.

Figure 3 shows the normalized IMD for the two samples as a function of the circulating power. The IMD signal of the oxygenated sample is more than 30-dBm lower than that of the other sample. This clearly shows that following a careful growth process and applying subsequent oxygen annealing can improve the microwave nonlinearity, as previously reported.[11,12] We have good reasons to assume that the differences are due to film quality and are not caused by substrate effects.

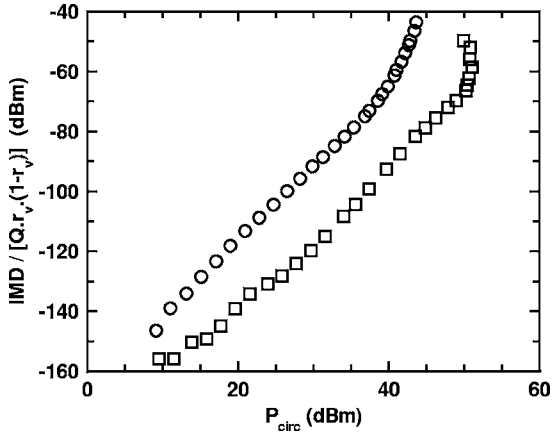

FIG. 3. The difference at $t=T/T_c=0.46$ between the levels of IMD for the baseline sample SP3 on $LaAlO_3$ (circles) and the reference sample D on MgO that was annealed (squares).

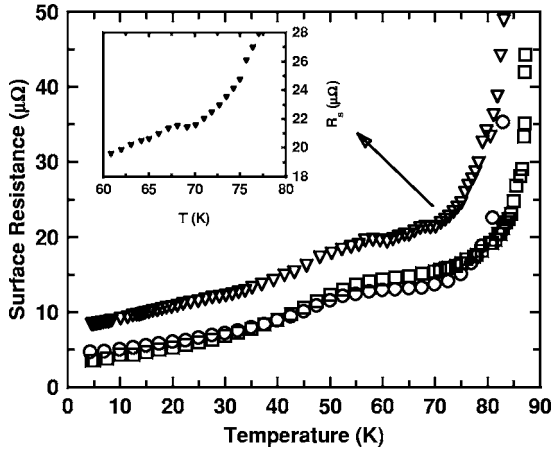

FIG. 4. Linear surface resistance $R_s(T)$ at 1.5 GHz and −16 dBm as a function of temperature for the set of samples deposited by sputtering onto $LaAlO_3$ substrates. The sample with a 40-nm $Y_{0.7}Ca_{0.3}Ba_2Cu_3O_{7-\delta}$ overlayer SP2 (triangles) has a higher linear R_s than the one with a 20-nm overlayer SP1 (circles) and the baseline SP3 (squares). The inset shows detail near 70 K for the 40-nm overlayer.

V. SPUTTERED FILMS ON $LaAlO_3$

As mentioned in Sec. III A, the two baseline samples on $LaAlO_3$ have an identical behavior, so the results of only one are presented. The penetration depth λ_0 and the critical temperature T_c obtained by microwave measurements are given in Table I (Ref. 29). The T_c of the samples matches that measured by dc resistivity.

From Table I, we see that the critical temperature is not affected by the presence of the Ca-rich layer. If Ca diffusion were uniform, as inferred from Berenov's steady-state results, the overall Ca concentration (~3–4%) should lead to a decrease of T_c of a few K that we do not observe, implying that grains contain little Ca. A change in the oxygen content of the film during the growth of the overlayer can also lead to a small variation of T_c. The penetration depths are comparable after deposition of the Ca-rich layer. The value of the penetration depth can be influenced by sources like the presence of defects or weak links or a broadening of the superconducting transition, as the method used to determine the penetration depth gives an average value.[29] Also shown is the low-power R_s.

A. Surface resistance versus temperature $R_s(T)$

The surface resistance $R_s(T)$ measured at 1.5 GHz and −16-dBm input power for this set of samples is presented in Fig. 4. All films exhibit a shoulder at 55 K, indicating that grains are free of Ca, which is localized adjacent to boundaries, adding no contribution to the intrinsic mean-free path in the grains.[9] Between 40 and 70 K, a slight improvement is observed after deposition of a 20-nm-thick $Y_{0.7}Ca_{0.3}Ba_2Cu_3O_{7-\delta}$ surface layer, but the deposition of a 40-nm-thick overlayer degrades R_s. This film also exhibits a broader superconducting transition than the two other films. This compares well with the results of Obara *et al.*[22,23]

We did not investigate the origin of the shoulder at T_c' ~75 K for the sample with a 40-nm overlayer. It could be indicative of a pseudogap[40] or even be the T_c of the overlayer. Moreover, the broad superconducting transition might reveal the presence of inhomogeneities, like green-phase YBCO (Y_2BaCuO_5) previously observed on the x-ray patterns and likely caused by corrosion.[41]

B. Nonlinear surface impedance $Z_s(I_{rf})$

The nonlinear contribution to the surface impedance $Z_s(I_{rf})$ is shown in Fig. 5. The rf current I_{rf} is calculated from the unloaded quality factor, input power, and the insertion loss.[42] As can be seen, the deposition of a 20-nm Ca-rich surface layer improves $R_s(I_{rf})$ and $\Delta X_s(I_{rf})$, with $I_p \approx 0.6$ A, to be compared with $I_p \approx 0.4$ A for the plain YBCO film, where I_p is the current corresponding to the field of flux penetration H_p (Ref. 39). The improvement of the nonlinear behavior shows that Ca substitution can under some circum-

TABLE I. Critical temperature T_c and penetration depth λ_0 of the samples on $LaAlO_3$ at 1.5 GHz.

Sample	t(YBCO) nm	t (overlayer) nm	T_c (μ wave) (K)	T_c (dc)	λ_0 nm	R_s $t=0.46$ $\mu\Omega$
SP1	400	20	87		218	8.85
SP2	400	40	89.5	89.7	235	15.68
SP3	400	0	88.4		247	8.97

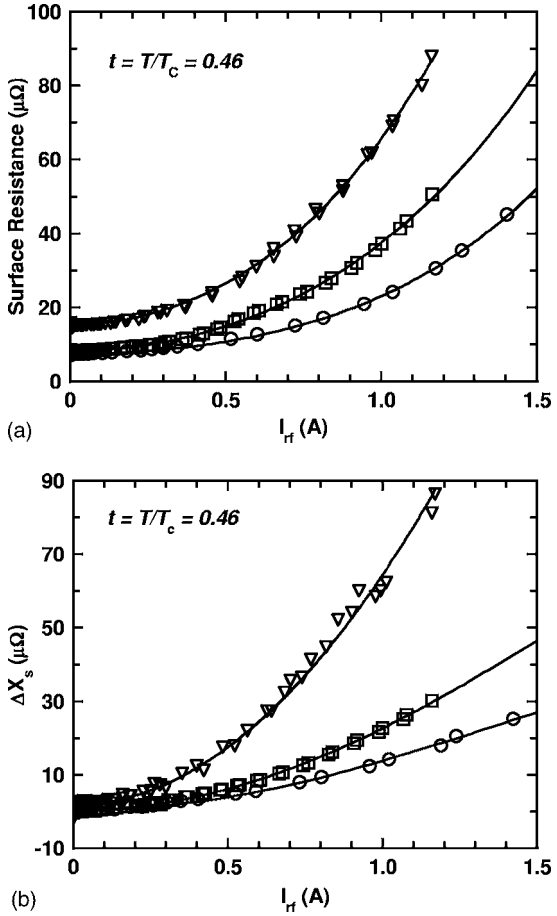

FIG. 5. Nonlinear surface impedance $Z_s(I_{\mathrm{rf}})$ as a function of the microwave current measured at $t=T/T_c=0.46$ for the set of samples on $LaAlO_3$. The nonlinear surface resistance $R_s(I_{\mathrm{rf}})$ is plotted on the upper graph and the variation of the reactance $\Delta X_s(I_{\mathrm{rf}})$ on the lower graph. The lines are a polynomial fit of the data at the fourth order in the microwave current I_{rf}. The sample SP2 (triangles) has a pronounced curvature of $R_s(I_{\mathrm{rf}})$ and $\Delta X_s(I_{\mathrm{rf}})$, whereas SP1 (circles) has a better nonlinear behavior than the baseline SP3 (squares).

stances be used to enhance the microwave power-handling capability of a YBCO film. The opposite situation is observed in the case of the sample with a 40-nm-thick surface layer, which has the lowest power-handling capability, with $I_p \approx 0.3$ A. As in the low-power regime, the results with this second film give a limitation on the thickness and the substitution level of the overlayer.

C. Intermodulation distortion products

IMD measurements were used for additional studies of the nonlinear behavior of the films. Figure 6 shows the results. A tone separation smaller than 1/10 the 3-dB bandwidth of the resonant curve was used. The normalization corresponding to Eq. (3) for different insertion loss and Q values of the resonators is applied to compare the IMD response of the three films.[35,36] The lowest level of IMD is measured for the sample with a 20-nm-thick $Y_{0.7}Ca_{0.3}Ba_2Cu_3O_{7-\delta}$ surface layer. The difference between the values of this sample and of the baseline sample is about

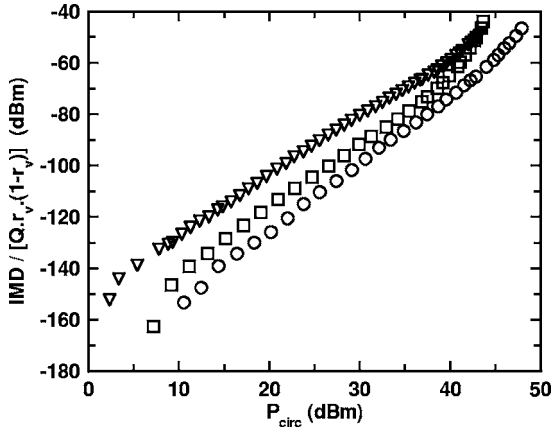

FIG. 6. Results of the IMD measurements at $t=T/T_c=0.46$ for the set of samples on $LaAlO_3$ substrates. The results are scaled by the unloaded quality factor Q and the insertion losses factor $r_v(1-r_v)$. The output power at the lower intermode is plotted as a function of the circulating power P_{circ}. The symbols are as follows: baseline SP3 (squares), SP1 (circles), and SP2 (triangles).

8 dB at 25-dBm circulating power, which implies that a thin Ca-rich overlayer improves the IMD slightly. At this circulating power, the sample with a 40-nm-thick $Y_{0.7}Ca_{0.3}Ba_2Cu_3O_{7-\delta}$ surface layer has a level of IMD that is about 12 dB higher than the level of the baseline sample. This result is consistent with the linear R_s (Sect. IV A) (Ref. 35) and $Z_s(I_{\mathrm{rf}},T)$ (Ref. 32) (Sec. IV B). These results are qualitatively consistent with the concept that the IMD output power is a function of the nonlinear a_{Xs} and a_{Rs} contribution as defined in Eq. (1).

D. Results after etching of the overlayer

To further determine the influence of the Ca-rich surface layer on the results presented above, we ion-etched a thin layer (~50 nm) off the surface of each sample to provide information on the surface processes and the diffusion of Ca atoms.

1. Influence on the linear surface resistance $R_s(T)$

Figure 7 presents the $R_s(T)$ for each sample, before and after etching. After etching, all samples are characterized by nearly the same R_s. A slight decrease in $R_s(T)$ of unknown origin is observed for the baseline. The decrease is largest for the sample that had a 40-nm-thick $Y_{0.7}Ca_{0.3}Ba_2Cu_3O_{7-\delta}$ surface layer, with $\Delta R_s(50\mathrm{K}) \sim 4\ \mu\Omega$. The difference before and after etching for the baseline is $\Delta R_s(50\ \mathrm{K}) \sim 1.4\ \mu\Omega$ and for the film with a 20-nm-thick overlayer we observe $\Delta R_s(50\ \mathrm{K}) \sim 2.8\ \mu\Omega$. The results are consistent with the absence of Ca diffusion into the grains, as already inferred from the T_c's of this set of samples, and inconsistent with the report of Berenov[16,17] for steady-state diffusion conditions.

2. Influence on the nonlinear surface impedance and the IMD products

Figure 8 presents the change of the nonlinear surface resistance and reactance after etching. No significant change

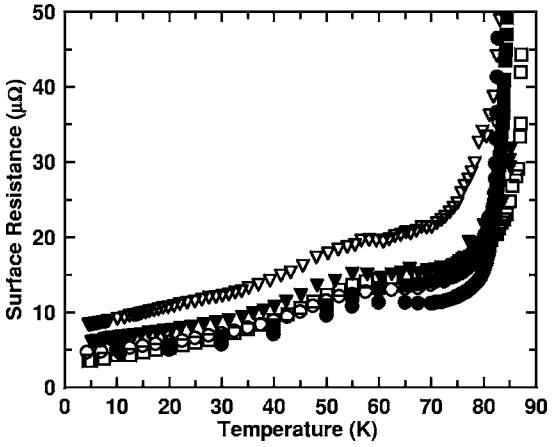

FIG. 7. Linear surface resistance $R_s(T)$ at −16 dBm as a function of temperature for the set of samples deposited on $LaAlO_3$ substrates before (open symbols) and after etching (filled symbols) off a 50-nm thickness from the surface. All the curves tend to be closer together after etching. The symbols are as follows: baseline SP3 (squares), SP1 (circles), and SP2 (triangles). The measurement was done at 1.5 GHz.

appears in the nonlinear components. All samples exhibit a slightly more pronounced nonlinear behavior after etching. A $\sim 10\%$ reduction in I_p is observed and could result from corrosion of the surface, likely to occur after etching.[43]

After etching, IMD levels for all samples increased, as much as 15–20 dB at $P_{\mathrm{circ}}=20$ dBm for one of the samples (Fig. 9). The differences between the samples are conserved before and after etching. The difference between the baseline and the sample with a 20-nm overlayer is still about 8 dB at intermediate power (25 dBm) after etching, and it is still about 12 dB with the sample that had a 40-nm overlayer. As previously mentioned, corrosion may have occurred during etching.

VI. FILMS COEVAPORATED ONTO MgO

All films from this set are slightly overdoped with oxygen. We note that the oxygen annealing may give the steady conditions for Ca diffusion as in Berenov's experiment. The dc magnetization was used to determine the transition temperature and the critical current of the films. The values are summarized in Table II. The T_c given in Table II was extracted from microwave measurement and it agrees with the T_c derived from the dc magnetization measurement.

A lower T_c is observed for the films that had a surface layer deposited on top. These samples were cooled in an oxygen atmosphere after deposition of the surface layer. A slight variation in the oxygen content may have been induced while sample D did not experience this step. We also observed that sample B, which still has a 40-nm-thick $Y_{0.7}Ca_{0.3}Ba_2Cu_3O_{7-\delta}$ surface layer, exhibits the lowest critical temperature. This can be the sign of Ca diffusion.

The j_c of the films that had the surface treatments are almost identical, except for sample A at 60 K. The reference sample D has the highest j_c at 60 and 77 K. This indicates that the growth of a YBCO overlayer by PLD, at about 60 °C above their growth temperature, has slightly degraded their superconducting properties. In addition, etching the overlayer may have affected the surface.

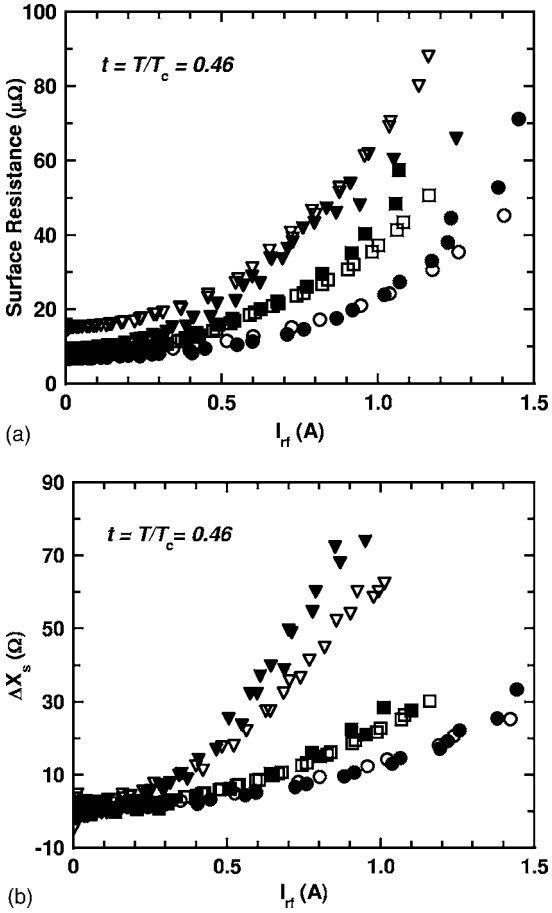

FIG. 8. A change in the nonlinear surface resistance $R_s(I_{\mathrm{rf}})$ of the set of samples on $LaAlO_3$ before (open symbols) and after etching (filled symbols) off 50 nm from the surface measured at $t=T/T_c=0.46$. The symbols are as follows: baseline SP3 (squares), SP1 (circles), and SP2 (triangles).

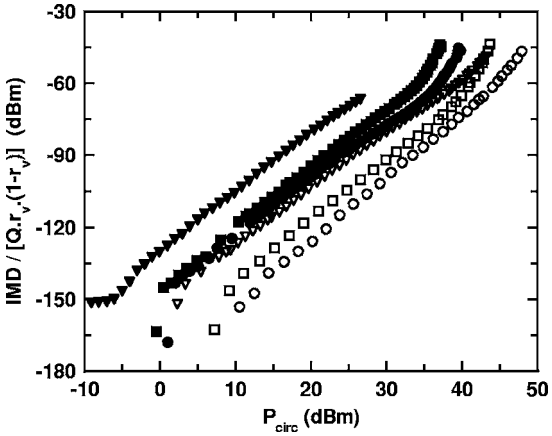

FIG. 9. Change in the IMD level measured before (open symbols) and after etching (filled symbols) for the set of samples on $LaAlO_3$ at $t=T/T_c=0.46$. The symbols are as follows: baseline SP3 (squares), SP1 (circles), and SP2 (triangles).

TABLE II. Characteristic values of the four evaporated samples on MgO at $t=T/T_c=0.46$.

Sample	t(YBCO) nm	t(overlayer) nm	O_2 anneal	T_c K	J_c(60K) (A cm^{-2})	J_c(77K) (A cm^{-2})	λ_0 nm	R_s $t=0.46$ $\mu\Omega$
A	350	40 (YBCO) (removed)	2	85	1.05×10^7	1.81×10^6	176	6.37
B	350	40 (YCaBCO)	2	83.4	1.28×10^7	1.78×10^6	182	7.60
C	350	40 (YCaBCO) (removed)	2	84.7	1.22×10^7	1.88×10^6	189	7.32
D	350	0	2	89.2	1.46×10^7	3.72×10^6	189	5.68

A. Surface resistance versus temperature $R_s(T)$

The variation of the effective surface resistance with temperature at 2.3 GHz and at low power is presented in Fig. 10. A local maximum is observed for each sample around 20 K because the stripline resonator yields an effective $R_s=R_s^{\text{film}}+G\tan\delta$, where G is a geometric factor and $\tan\delta$ is the loss tangent of the dielectric. The second term, related to the losses in the dielectric, is usually negligible compared to $R_s^{\text{film}}(T)$ as for the previous set of samples deposited on $LaAlO_3$. However, for MgO at low T, this term becomes important because losses increase due to the presence of impurities, and the MgO becomes nonlinear as a function of the microwave electric field.[44,45] The local maximum below 20 K is a consequence of these effects in the MgO. At $T\geqslant 60$ K, the R_s of the YBCO, R_s^{film}, dominates.

As can be seen in Fig. 10, the reference sample D, which did not have any surface treatment, has the lowest linear R_s. By comparison, the sample A, which initially had a YBCO overlayer on its surface, exhibits a slightly higher R_s. This suggests that the deposition of the surface layer (effectively equivalent to a high-temperature anneal) or its removal had a damaging effect. The critical temperature of the sample A also indicates a change in the oxygen content of this sample by comparison with the reference sample D. In addition, the annealing done on this set produced steady-state conditions for the diffusion of Ca atoms, in contrast to the dynamic conditions in the case of the set on $LaAlO_3$.

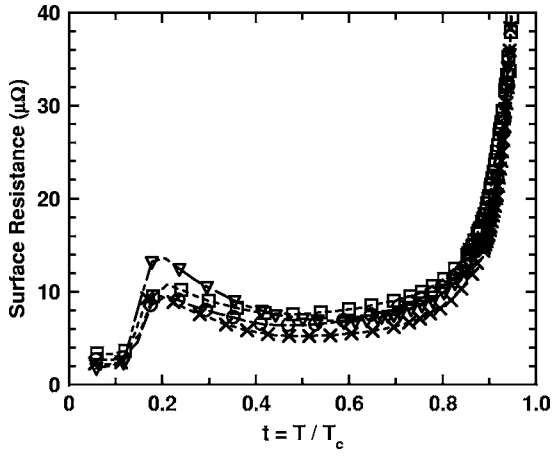

FIG. 10. Linear surface resistance $R_s(t)$ at 2.3 GHz and −16 dBm as a function of the reduced temperature $t=T/T_c$ for the set of samples deposited onto MgO substrates. A local peak caused by losses in the MgO is observed around 20 K. The samples are plotted as follows: A (circles), B (squares), C (triangles), D (crosses).

The increase of R_s is more pronounced for the two samples that have been doped via Ca substitution, the largest for the sample that still has the Ca-doped layer on its surface. This result is to be compared with the set of sputtered samples on $LaAlO_3$, where a 40-nm-thick $Y_{0.7}Ca_{0.3}Ba_2Cu_3O_{7-\delta}$ surface layer also leads to an increase of the linear R_s. The increase in the linear R_s is still significant for sample C that had this overlayer removed. The thickness that was removed corresponds approximately to that deposited. This suggests that Ca atoms diffused into the YBCO film. Corrosion and other etching-related effects might also lead to this result.

B. Nonlinear surface impedance $Z_s(I_{\text{rf}})$

The results of the nonlinear $R_s(I_{\text{rf}})$ and the change in the surface reactance $\Delta X_s(I_{\text{rf}})$ are plotted in Fig. 11 as a function of the microwave current I_{rf} in the resonator. Except in the low-power-R_s (linear) regime, the $R_s(I_{\text{rf}})$ curves do not show significant differences. As observed the different surface treatments applied to sample A and C do not have a significant impact on the nonlinear components of the surface impedance, in contrast to the linear surface impedance. The curvature of the surface reactance $\Delta X_s(I_{\text{rf}})$ is slightly more pronounced for the Ca-doped sample B. For a circulating current of 1 A, ΔX_s for this sample has increased by approximately 7 $\mu\Omega$ more than for the three other samples, which corresponds to an increase of 50% after doping compared to the samples from the same set. The 40-nm-thick Ca-substituted overlayer thus causes larger nonlinearities of the surface impedance, similar to that previously observed with the set of samples deposited on $LaAlO_3$.

C. IMD results

The normalized IMD data are presented in Fig. 12. Below approximately 20-dBm circulating power, the IMD level might be influenced by the nonlinearities of the MgO substrate. In the range of circulating power from 20 to 50 dBm, the sample with a Ca-rich overlayer has a 6-10- dB higher IMD signal than the two samples that were not treated with Ca, and the sample that has the Ca-rich overlayer removed has an IMD level that is 4-dB higher than the unsubstituted samples, which might result from Ca diffusion into the YBCO film or the presence of a thin Ca-substituted layer at the surface. The two plain YBCO samples have an identical

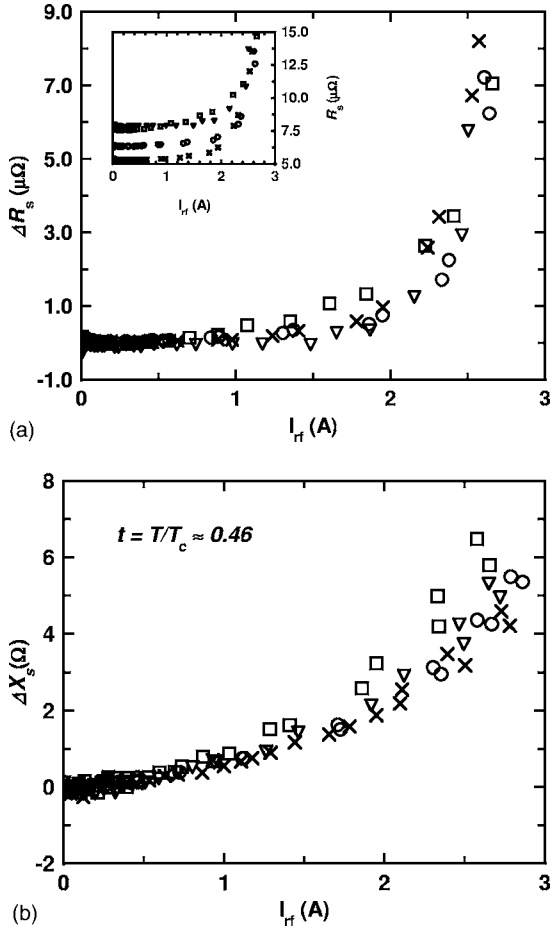

FIG. 11. Nonlinear surface impedance $Z_s(I_{\mathrm{rf}})$ as a function of the microwave current measured at $t=T/T_c=0.46$ and at 2.3 GHz for the set of samples on MgO. The variation of nonlinear surface resistance $R_s(I_{\mathrm{rf}})$ is plotted on the upper graph and the variation of the reactance $\Delta X_s(I_{\mathrm{rf}})$ on the lower graph. The inset is the nonlinear $R_s(I_{\mathrm{rf}})$. The samples are plotted as follows: A (circles), B (squares), C (triangles), D (crosses).

behavior over the whole power range, indicating that the surface processes applied to A had little effect on the nonlinearities.

These results are consistent with the idea that the IMDs depend on the nonlinear contribution of the surface impedance (Fig. 11), as the Ca-substituted sample shows a higher level of intermodulation. The results are also consistent with the previous observation of the different surface treatments having only a small effect on the nonlinearities compared to the linear components (Fig. 11), as the two plain YBCO samples are indistinguishable.

VII. DISCUSSION OF THE EFFECT OF THE Ca SUBSTITUTION

Several reasons are considered to explain the degradation of the microwave linear and nonlinear properties after deposition of a 40-nm-thick 30%-substituted surface layer. As previously confirmed by the work of Obara *et al.*,[22,23] the thickness of the surface layer is an important parameter that

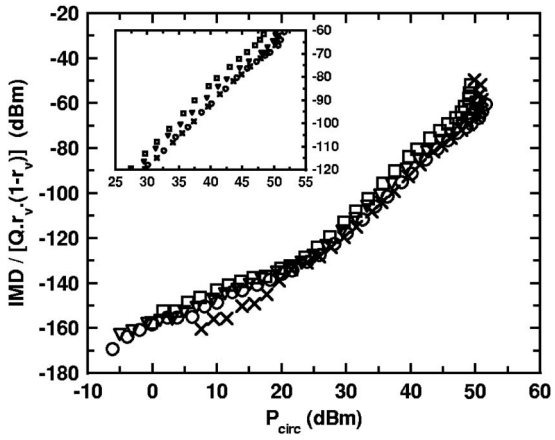

FIG. 12. Results of the IMD measurements as a function of the circulating power P_{circ} and at $t=T/T_c=0.46$ and 2.3 GHz for the set of samples on MgO substrates. The results are scaled by Q and the insertion loss factor $r_v(1-r_v)$. The samples are plotted as follows: A (circles), B (squares), C (triangles), D (crosses).

can lead to an improvement or a degradation of the linear microwave properties. In their study, the surface layer was substituted with 20% Ca, which may explain why they observed an improvement of the linear $R_s(T)$ up to higher thicknesses than those used in our study. Our results for the linear $R_s(T)$ of the set of samples on $LaAlO_3$ are in agreement with those of Obara. In our study we extend the investigation to the nonlinear $Z_s(I_{\mathrm{rf}},T)$. More generally, our results are in agreement with the variation of the critical current density j_c measured by Hammerl *et al.*[2] as a function of the thickness of the overlayer. With the same substitution level (30%), an increase of j_c by nearly two times was observed for a thickness of 20 nm, followed by a decrease for a larger thickness of the overlayer. With a 40-nm-thick surface layer, their j_c was approximately the same as that without an overlayer, but their film contained high-angle GBs that helped the diffusion of the Ca atoms.

A thickness of 20 nm leads to an improvement, probably resulting from Ca diffusion in the GBs, while a surface layer of larger thickness behaves more like a poor quality film. The quality of the underlying YBCO film is also of particular importance, as it regulates the diffusion of the Ca atoms. Thus, a noticeable improvement in linear R_s was observed with the film of fair quality deposited onto $LaAlO_3$ that received a 20-nm-thick $Y_{0.7}Ca_{0.3}Ba_2Cu_3O_{7-\delta}$ surface layer. The set on MgO is of higher quality and may not offer as many diffusion paths as the set on $LaAlO_3$. However, diffusion may have taken place for the set on MgO as the oxygen annealing favors steady conditions for Ca diffusion. Both sets of films showed worse performance when a 40-nm-thick $Y_{0.7}Ca_{0.3}Ba_2Cu_3O_{7-\delta}$ surface layer is used.

It has been shown that the superconducting properties of homogeneously substituted films degrade with high levels of Ca substitution, either because of substitution on the Ba sites,[4,6,8] oxygen vacancies, or structural disorder. In the microwave range, the linear R_s strongly increases as the Ca substitution is enhanced above 10%.[21]

The surface layer deposited on top of the YBCO sample can, to a good approximation, be considered as a uniformly

TABLE III. Real and imaginary part of the conductivity and R_s at $t=T/T_c=0.4$ and 2.3 GHz for the samples A, C, and D. The conductivities σ_1 and σ_2 are derived from measurements using Eq. (9) and the expression of the penetration depth. For the YBCO underlayer of the sample B and the Ca-doped layer, σ_1 and σ_2, were calculated using Eqs. (7) and (8).

	A	B (composite)	B (YBCO underlayer)	C	D	Ca-doped layer
σ_1(S m)	6.82×10^6	7.25×10^6	6.22×10^6	6.23×10^6	4.98×10^6	1.23×10^7
σ_2(S m)	1.72×10^9	1.60×10^9	1.64×10^9	1.48×10^9	1.51×10^9	1.28×10^9
$R_s(\mu\Omega)$	6.37	7.59	6.24	7.32	5.68	17.96

substituted thin film, whose properties can be extracted by an analytical approach. This is the approach presented below.

To obtain the properties of the surface layer, the set of samples deposited onto MgO is used, because the experimental procedure allows a comparison between the film with the Ca-rich top layer and similar films that either had the Ca-rich top layer removed or a YBCO top layer removed. This will help to discriminate among surface and substitution processes.

From the change in the complex conductivity $\sigma=\sigma_1-i\sigma_2$ after doping, which can be calculated from the microwave measurements, conclusions on the quasiparticle density n_n and the Cooper-pair density n_s can be drawn, utilizing[46]

$$\sigma_1 = \frac{n_n e^2 \tau}{m(1+\omega^2\tau^2)}, \tag{4}$$

$$\sigma_2 = \frac{n_s e^2}{\omega m} + \frac{n_n e^2 \tau^2 \omega^2}{\omega m(1+\omega^2\tau^2)}, \tag{5}$$

where m is the effective mass of the charge carriers, e is the electrical charge, ω the angular frequency of the microwave current, and τ the quasiparticle relaxation time. The σ_1 is a linear function of the quasiparticle density [Eq. (4)], whereas σ_2 is related to the superconducting carrier density [Eq. (5)]. At microwave frequencies, the second term in σ_2 is usually negligible. From the value of the effective penetration depth, the R_s of the film that has a Ca-rich surface layer, and the one that had a YBCO surface layer removed, the conductivity of the Ca-substituted surface layer and its R_s were extracted with the assumption that the underlying YBCO is identical. The inductance and the resistance per unit length of the doped film can be written as the sum of two contributions from the YBCO film and the Ca-rich layer.[47] The rf current distribution can be considered, to a good approximation, to be uniform over the thickness of the film because $\lambda \sim t/2$. In that case, we can write

$$\int_{t_{layer}} \int_{width} |j|^2 \, dS = t_{layer} \int_{width} |j|^2 \, dw \tag{6}$$

and the integral over the width is the same for each layer. This analysis is implemented for the low-power range, which corresponds to small rf currents. Considering also that both samples have the same geometrical inductance, the effective penetration depth of the Ca-substituted layer can be extracted by using the expression for the kinetic inductance,[48]

$$L = \frac{\mu_0}{|I|^2}\left(\int_{t_{YBCO}} \int_{width} (\lambda_L^{YBCO})^2 |j|^2 \, dS + \int_{t_{Y(Ca)BCO}} \int_{width} (\lambda_L^{Y(Ca)BCO})^2 |j|^2 \, dS \right), \tag{7}$$

where λ_L is the penetration depth, t_i is the layer thickness, and dS refers to the cross section of the strip. The resistance per unit length is given by

$$R = \frac{1}{|I|^2}\left(\int_{t_{YBCO}} \int_{width} \frac{\sigma_1^{YBCO}}{(\sigma_2^{YBCO})^2} |j|^2 \, dS + \int_{t_{Y(Ca)BCO}} \int_{width} \frac{\sigma_1^{Y(Ca)BCO}}{(\sigma_2^{Y(Ca)BCO})^2} |j|^2 \, dS \right). \tag{8}$$

The conductivity σ_2 is known from $\lambda_L=(\omega\mu_0\sigma_2)^{-1/2}$. Then, from the resistance per unit length, the quasiparticle conductivity σ_1 is found, which provides an estimate of R_s for the overlayer.

$$R_s = \frac{\omega^2 \mu^2 \sigma_1 \lambda_L^3}{2}. \tag{9}$$

The results are summarized in Table III for one representative temperature.

The σ_1 is larger for sample B with the Ca-substituted overlayer still present (B composite), and even larger for the layer itself than for the other samples. This leads to higher R_s [Eq. (9)]. One could argue that the disorder caused by the presence of the Ca could decrease the scattering time and thereby increase the scattering rate and the real part of the conductivity. Ca inside the grains acts as a weak scatterer, reducing the mean free path and consequently the scattering time.[9,49] In addition, the shoulder, characteristic of intrinsic scattering,[9] observed on the $R_s(T)$ variation for the set on $LaAlO_3$ (Fig. 7), if present for the set on MgO, would be hidden by the MgO losses, preventing knowledge of the Ca content of the grains. Another explanation for the larger σ_1 is that Ca substituted on the Ba site. In that sense, the Cooper-pair conductivity σ_2 does not seem to change and even seems to be reduced for the surface layer, which enforces the idea that substitution on Ba site happened, as the density of states only increases if Ca substitutes for Y. It should be noted that microwave measurements lead to an effective average penetration depth that includes some contribution of weak links and other defects most likely to be present at the interface

Y(Ca)BCO/YBCO in the case of the doped sample. We expect, however, that the contribution of the interface to λ is negligible compared to that of the Ca substitution.

Fisher *et al.*[4] and Gasumyants *et al.*[50] proposed a change in the distribution between Cooper pairs and quasiparticles from measurements of the normal-state thermoelectric power of Ca-doped and undoped YBCO films. Other studies have proven that the density of superelectrons n_s effectively reaches a maximum and then decreases as a function of the number of holes p per CuO_2 plane, as observed in the superconducting state from measurement of the magnetic penetration depth for Hg-1201 powder using low-field ac susceptibility[51] and also in the case of $Y_{0.8}Ca_{0.2}Ba_2Cu_3O_{7-\varepsilon}$ and Tl-1212 from transverse field muon spin rotation.[52] The value of p is generally determined using the universal relation $p=0.16\pm[(1-T_c/T_{c,\max})/82.6]^{1/2}$ (Ref. 53) and room-temperature thermoelectric power measurements,[51,52] and the universal formulation cannot be used in our case, as the Ca-substituted film is in an overlayer, and its T_c is unknown. Nevertheless, the doping level of the Ca-substituted surface layer surely corresponds to $p>p_{\mathrm{crit}}$, where p_{crit} gives the maximum n_s. The overlayer was indeed doped from Ca substitution and oxygen annealing. This film is expected to be strongly overdoped and effectively have $p>p_{\mathrm{crit}}$. The variation observed in the real part of the conductivity (Table III) may indicate that the quasiparticle density increased with doping and at the same time the Cooper pair density decreased. A change in the distribution of the carriers between Cooper pairs and quasiparticles may occur as a consequence of disorder in the CuO chains and substitution on the Ba site, when the doping rate exceeds some threshold level. Such redistribution shows up in the microwave complex conductivity. In addition, the substitution could modify the density of holes in the CuO chains.[4,54] If substitution effectively takes place on the Y site, due to its size Ca reduces the interlayer coupling strength between CuO_2 planes, resizes the CuO chains, and may also act on the apical O (Ref. 7), all of which could change the distribution of the carriers. However, if we also consider substitution on the Ba site as proposed in this paper, we surely can expect a carrier redistribution to arise from disorder in the CuO chains. If that is correct, this measurement provides an additional confirmation of the hypothesis of a redistribution of the carriers.

VIII. SUMMARY AND CONCLUSIONS

The microwave properties of Ca-doped YBCO films were characterized by studying two sets of samples deposited by different methods and on different substrate materials. Doping was realized by using 30%-Ca-substituted surface layers. An improvement in linear R_s was observed for one sample when the thickness of the surface layer was 20 nm. With a 40-nm-thick overlayer, linear and nonlinear microwave properties are degraded. These results are in good agreement with previous linear microwave characterizations and also with the observation by Hammerl *et al.*[2] that the critical current density decreases when the surface layer thickness exceeds a certain value that also depends on the substitution level. A tradeoff between the thickness of the overlayer and the level of substitution seems clear. In this study, we conclude that the degradation is related to the high substitution level of the surface layer, which leads to poorer superconducting properties. According to previous studies, the degradation of the superconducting and microwave properties could result from disorder and substitution on the Ba site with a high level of Ca substitution. A comparison of the values of the microwave conductivity of the doped layer and the film leads us to propose a carrier redistribution.

We also confirm the importance of the oxygen level on the microwave nonlinearity. Samples that are optimally doped or slightly overdoped generate lower IMD signals and can handle higher microwave power before becoming nonlinear.

Another observation was related to the different effects of the surface processes in the linear and the nonlinear regime. Without taking into account the effects of doping, we observed that the surface processing (deposition and etching of a surface layer) increases the linear surface resistance but has little effect on the nonlinear contribution and the IMD. We observed a large shift of the IMD level after etching for one set of samples that is not reflected in the nonlinear surface impedance, whereas the difference among the sample remains constant. Thus, the correlation with the measurement of ΔZ_s does not seem to hold. These observations show that the relation between surface impedance and IMD needs further investigation, which is currently in progress.[55]

ACKNOWLEDGMENTS

The authors thank J. Halbritter and S.-H. Park for fruitful discussions. R. P. Koniezcka and D. Baker are acknowledged for assistance with fabrication and measurement. We thank G. Fitch for help with automation of the measurement. The work at Lincoln Laboratory was supported by the Air Force Office of Scientific Research (AFOSR). D. Seron was supported at MIT by the AFOSR and by the Délégation Générale de l'Armenent (DGA, France) under Contract No. 986083038. G. Hammerl and J. Mannhart acknowledge support by the BMBF (13N6918A) and the DFG (SFB484). The work at QinetiQ was supported by the UK MOD Corporate research program. M. Hein was supported in part by the European Office of Aerospace Research and Development, AFOSR/AFRL, under Contract No. F61775-01-WE033.

[1] D. E. Oates, S.-H. Park, D. Agassi, and G. Koren, Supercond. Sci. Technol. **17**, S290 (2004).
[2] G. Hammerl, A. Schmehl, R. R. Schulz, B. Goetz, H. Bielefeldt, C. W. Schneider, H. Hilgenkamp, and J. Mannhart, Nature **407**, 162 (2000).
[3] J. Mannhart, H. Bielefeldt, B. Goetz, H. Hilgenkamp, A. Schmehl, C. W. Schneider, and R. R. Schulz, Physica C **341-348**, 1393 (2000).
[4] B. Fisher, J. Genossar, C. G. Kuper, L. Patlagan, G. M. Reisner, and A. Knizhnik, Phys. Rev. B **47**, 6054 (1993).
[5] A. Manthiram, S. J. Lee, and J. B. Goodenough, J. Solid State Chem. **73**, 278 (1988).
[6] S. I. Schlachter, W. H. Fietz, K. Grube, Th. Wolf, B. Obst, P. Schweiss, and M. Kläser, Physica C **328**, 1 (1999).
[7] C. H. Hsieh, C. N. Chang, S. B. Lee, H.-C. I. Kao, and C. H. Chin, Physica C **384**, 314 (2003).
[8] G. Böttger, H. Schwer, E. Kaldis, and K. Bente, Physica C **275**, 198 (1997).
[9] E. Gaganidze and J. Halbritter, Supercond. Sci. Technol. **17**, 1 (2004).
[10] J. T. Kucera and J. C. Bravman, Phys. Rev. B **51**, 8582 (1995).
[11] D. E. Oates, M. A. Hein, P. J. Hirst, R. G. Humphreys, G. Koren, and E. Polturak, Physica C **372-376**, 462 (2002).
[12] D. E. Oates, S. H. Park, M. A. Hein, P. J. Hirst, and R. G. Humphreys, IEEE Trans. Appl. Supercond. **13**, 311 (2003).
[13] Y. M. Habib, C. J. Lehner, D. E. Oates, L. R. Vale, R. H. Ono, G. Dresselhaus, and M. S. Dresselhaus, Phys. Rev. B **57**, 13833 (1998).
[14] H. Xin, D. E. Oates, G. Dresselhaus, and M. S. Dresselhaus, Phys. Rev. B **65**, 214533 (2002).
[15] J. Mannhart and H. Hilgenkamp, Mater. Sci. Eng. B **56**, 77 (1998).
[16] A. V. Berenov, R. Marriott, S. R. Foltyn, and J. L. MacManus-Driscoll, IEEE Trans. Appl. Supercond. **11**, 3780 (2001).
[17] A. V. Berenov, C. Farvacque, X. Qi, J. L. MacManus-Driscoll, D. MacPhail, and S. R. Foltyn, Physica C **372-376**, 1059 (2002).
[18] K. Guth, H. U. Krebs, H. C. Freyhardt, and Ch. Jooss, Phys. Rev. B **64**, 140508(R) (2001).
[19] M. A. Schofield, M. Beleggia, Y. Zhu, K. Guth, and C. Jooss, Phys. Rev. Lett. **92**, 195502 (2004).
[20] G. Hammerl, H. Bielefeldt, B. Goetz, A. Schmehl, C. W. Schneider, R. R. Schulz, H. Hilgenkamp, and J. Mannhart, IEEE Trans. Appl. Supercond. **11**, 2830 (2001).
[21] M. Lorenz, H. Hochmuth, M. Grudmann, E. Gaganidze, and J. Halbritter, Solid-State Electron. **47**, 2183 (2003).
[22] H. Obara, A. Sawa, H. Yamasaki, and S. Kosaka, Appl. Phys. Lett. **78**, 646 (2001).
[23] H. Obara, A. Sawa, K. Develos, H. Yamasaki, and S. Kosaka, Physica C **378-381**, 1419, (2002).
[24] A. C. Anderson, R. L. Slattery, D. E. Oates, and L. S. Yu-Jahnes, Lincoln Lab., Lexington, MA, 1993 Solid State Res. Quarterly Tech. Rep. Vol. 2, 1993, pp. 31–33.
[25] R. Humphreys, *Microwave Superconductivity*, NATO Science Series, Series E: Applied Sciences-Vol. 375, 55 (2001).
[26] D. Seron, D. E. Oates, A. C. Anderson, G. Hammerl, J. Mannhart, P. J. Hirst, R. G. Humphreys, and M. A. Hein, Supercond. Sci. Technol. **17**, S422 (2004).
[27] N. G. Chew, J. A. Edwards, R. G. Humphreys, J. S. Satchell, S. W. Goodyear, B. Dew, N. J. Exon, S. Hensen, M. Lenkens, G. Muller, and S. Orbach-Werbig, IEEE Trans. Appl. Supercond. **5**, 1167 (1995).
[28] D. E. Oates, A. C. Anderson, and P. M. Mankiewich, J. Supercond. **3**, 251 (1990).
[29] S. Revenaz, D. E. Oates, D. Labbé-Lavigne, G. Dresselhaus, and M. S. Dresselhaus, Phys. Rev. B **50**, 1178 (1994).
[30] J. C. Booth, L. R. Vale, R. H. Ono, and J. H. Claassen, J. Supercond. **14**, 65 (2001).
[31] T. Dahm and D. J. Scalapino, J. Appl. Phys. **81**, 2002 (1997).
[32] C. Collado, J. Mateu, and J. M. O'Callaghan, IEEE Trans. Appl. Supercond. **15**, 26 (2005).
[33] B. A. Willemsen, B. H. King, T. Dahm, and D. J. Scalapino, IEEE Trans. Appl. Supercond. **9**, 4181 (1999).
[34] A. V. Velichko, Supercond. Sci. Technol. **16**, 1 (2003).
[35] E. A. Vopilkin, A. E. Parafin, and A. N. Reznik, Tech. Phys. **45**, 214 (2000).
[36] R. G. Humphreys, M. A. Hein, and D. E. Oates, unpublished.
[37] Th. Kaiser, B. A. Aminov, A. Baumfalk, A. Cassinese, H. J. Chaloupka, M. A. Hein, S. Kolesov, H. Medelius, G. Muller, M. Perpeet, H. Piel, and E. Wikborg, J. Supercond. **12**, 343 (1999).
[38] J. Halbritter, J. Appl. Phys. **68**, 6315 (1990).
[39] P. P. Nguyen, D. E. Oates, G. Dresselhaus, M. S. Dresselhaus, and A. C. Anderson, Phys. Rev. B **51**, 6686 (1995).
[40] J. Halbritter, J. Supercond. **14**, 9 (2001).
[41] M. Regier, E. Keskin, and J. Halbritter, IEEE Trans. Appl. Supercond. **9**, 2375 (1999).
[42] D. E. Oates, in *Microwave Superconductivity*, NATO Science Series, Series E: Applied Sciences, edited by H. Weinstock and M. Nisenoff, 2001, Vol. 375, p. 117.
[43] E. Gaganidze, T. Kaiser, and J. Halbritter, Supercond. Sci. Technol. **17**, 601 (2004).
[44] M. A. Hein, D. E. Oates, P. J. Hirst, R. G. Humphreys, and A. V. Velichko, Appl. Phys. Lett. **80**, 1007 (2002).
[45] M. A. Hein, R. G. Humphreys, P. J. Hirst, S.-H. Park, and D. E. Oates, J. Supercond. **16**, 895 (2003).
[46] M. J. Lancaster, in *Microwave Superconductivity*, NATO Science Series, Series E: Applied Sciences, edited by H. Weinstock and M. Nisenoff, 2001, Vol. 375, p. 91.
[47] S. A. Zhou, *Electrodynamics of Solids and Microwave Superconductivity* (Wiley Interscience, New York, 1999), p. 482.
[48] D. M. Sheen, S. M. Ali, D. E. Oates, R. S. Withers, and J. A. Kong, IEEE Trans. Appl. Supercond. **1**, 108 (1991).
[49] J. Halbritter, J. Supercond. **16**, 833 (2003).
[50] V. E. Gasumyants, M. V. Elizarova, E. V. Vladimirskaya, and I. B. Patrina, Physica C **341-348**, 585 (2000).
[51] C. Panagopoulos, T. Xiang, W. Anukool, J. R. Cooper, Y. S. Wang, and C. W. Chu, Phys. Rev. B **67**, 220502(R) (2003).
[52] C. Bernhard, J. L. Tallon, Th. Blasius, A. Golnik, and Ch. Niedermayer, Phys. Rev. Lett. **86**, 1614 (2001).
[53] M. R. Presland, J. L. Tallon, R. G. Buckley, R. S. Liu, and N. E. Flower, Physica C **176**, 95 (1991).
[54] S. K. Bandyopadhyay, P. Sen, P. Barat, P. Mukherjee, A. Bhattacharyay, P. Rajasekar, P. Chakraborty, F. Caccavale, S. LoRusso, A. K. Ghosh, and A. N. Basu, Phys. Lett. A **226**, 237 (1997).
[55] D. Agassi (unpublished).